THE JOURNAL OF PHYSICAL CHEMISTRY A
A JOURNAL OF THE AMERICAN CHEMICAL SOCIETY

pubs.acs.org/JPCA

Article

Synthesis and Optical Characterization of a Rhodamine B Spirolactam Dimer

Brandy-Fey C. Stratton, Angelina J. Pierre, Elizabeth A. Riser, Nathan J. Grinalds, Charles W. Edwards, Anna M. Wohlwend, Jacob S. Bauer, Rachel J. Spera, Lauren S. Pferdmenges, Kaitlyn M. Griffith, Brandon W. Hunter, Petia Bobadova-Parvanova, Cynthia S. Day, Pamela M. Lundin,* and Keir H. Fogarty*

Cite This: *J. Phys. Chem. A* 2022, 126, 4211−4220

Read Online

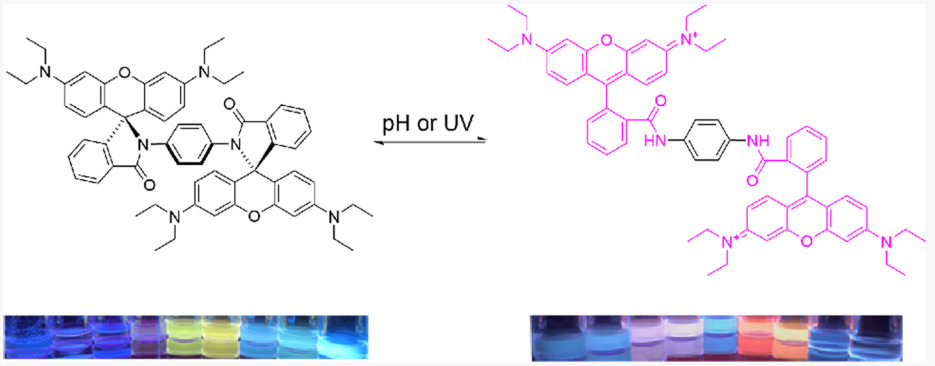

ABSTRACT: Amide derivatives of xanthene dyes such as rhodamine B are useful in a variety of sensing applications due to their colorimetric responses to stimuli such as acidity changes and UV light. The optical properties of these molecules can be influenced by intermolecular associations into dimeric structures, but the exact impact can be hard to predict. We have designed a covalently linked intramolecular dimer of the dye rhodamine B utilizing *p*-phenylenediamine to link the two dyes via amide bonds. The doubly closed spirolactam version of this dimer, **RSL$_2$**, is isolated as a colorless solid. Under acidic conditions or UV exposure, **RSL$_2$** solutions develop a pink color that is expected for the ring-opened form of the molecule. However, nuclear magnetic resonance (NMR) and single-crystal diffraction data show that the equilibrium still prefers the closed dimer state. Interestingly, the emission profile of **RSL$_2$** shows solvatochromic blue fluorescence. Control studies of model compounds with similar structural motifs do not display similar blue fluorescence, indicating that this optical behavior is unique to the dimeric form. This behavior may lend itself to applications of such xanthene dimers to more sophisticated sensors beyond those with traditional binary on/off fluorescence profiles.

INTRODUCTION

Rhodamine B is a common xanthene dye that has historically been used in dye lasers[1−4] and textile dyeing.[5] As our understanding of rhodamine B's chemical and photophysical properties has progressed, interest has grown in chemically modifying the basic structure of the dye to expand its utility in a variety of applications. One of the most studied modifications is the conversion of the carboxylic acid of rhodamine B into an amide, which can adopt two forms: a closed, spirolactam form in which the fluorescence of the xanthene core is quenched due to the disruption of conjugation, or an open form, which is fluorescent (Figure 1a). The transition from the closed to open form is sensitive to both pH[6−14] and ultraviolet illumination,[15−23] which enables the use of rhodamine spirolactams (RSLs) in sensing or other dye-activation on/off switching applications.

The pH-sensitive transition of RSLs between the closed, deprotonated form and the open, protonated form is dependent on substituent groups attached to the nitrogen of the amide.[7−14] Studies indicate that the kinetics and pKa values of RSLs are governed by both the sterics[9,13,14] and electron-withdrawing/donating nature[8,10,11,14] of the amide substituents. In general, increasing the size and electron-withdrawing character of the substituent groups shifts pKa values to higher numbers.[14] In addition, smaller, electron-withdrawing groups result in faster ring-opening kinetics and

Received: April 18, 2022
Revised: June 8, 2022
Published: June 24, 2022

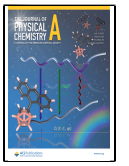

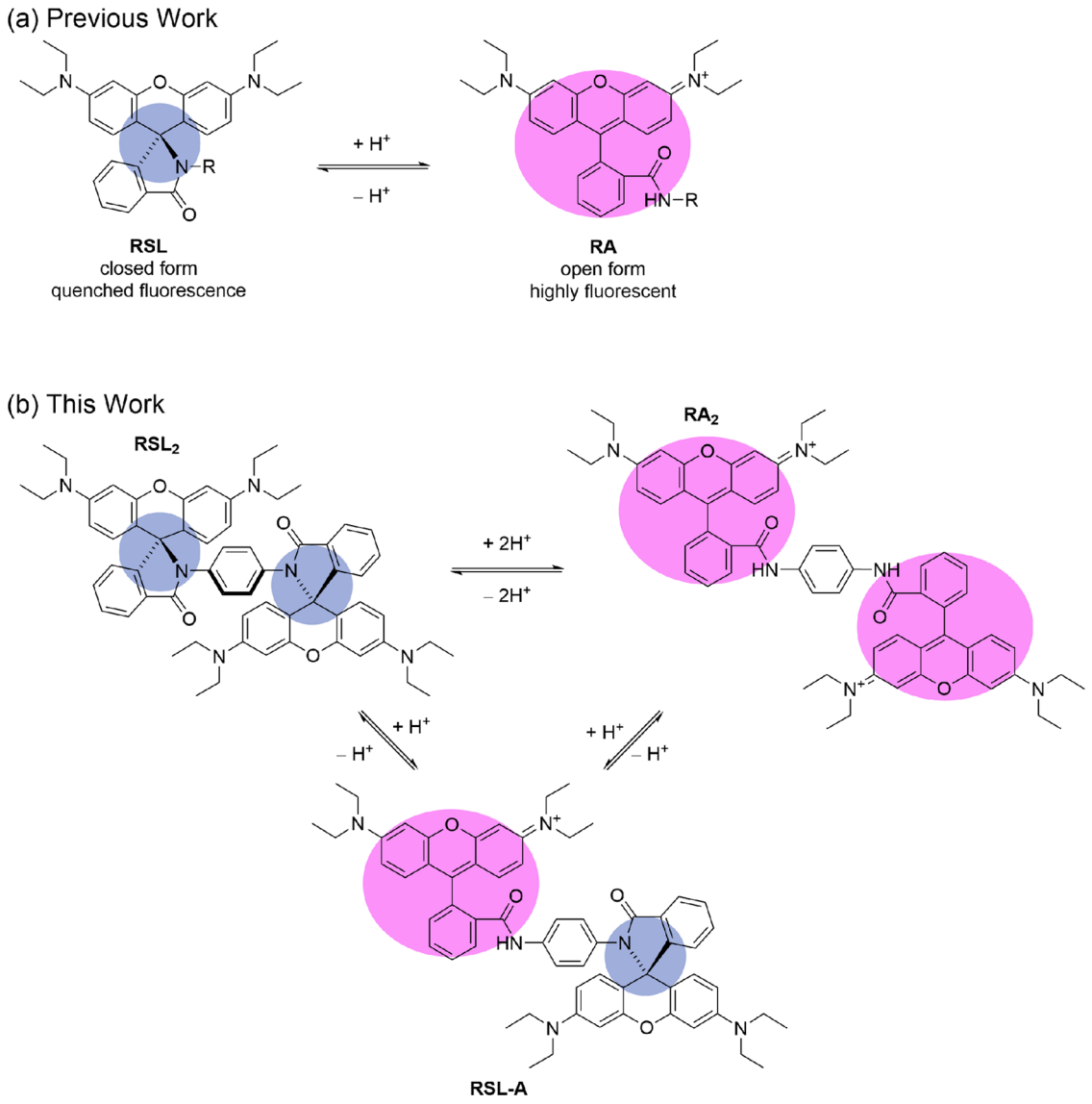

Figure 1. (a) Equilibrium between the closed and open forms of generic rhodamine B spirolactams. (b) Potential equilibria between the doubly closed (**RSL$_2$**), doubly opened (**RA$_2$**), and singly opened and singly closed (**RSL-A**) form of the rhodamine B dimer investigated in this work.

favor the open form of the spirolactam in equilibrium.[13] The most common application of pH-sensitive RSL probes is as lysosome markers in cells, as the low pH of the lysosome environment, relative to the surrounding cellular environment, leads to turn-on of RSL probe fluorescence.[11,12]

Photoswitching is another mechanism of RSL control between closed and open forms. Ring-opening is observed when RSLs are exposed to light in the range of ∼250 to 400 nm.[15] As with pH, the kinetics of ring-opening is influenced by the sterics and electron-withdrawing/donating nature of substituent groups attached to the nitrogen of the amide.[16,19,23] In addition, ring-opening kinetics are dependent on solvent effects, with solvent acidity and polarity playing a role.[15,16,19,20] Acidic solvents favor the formation of the open form of RSLs,[15,16,19] while the effect of solvent polarity is more variable.[20] RSL photoactivation has been used in a variety of applications, most notably in super-resolution microscopy.[17,18,21,23] Other applications of RSL photoswitching include volumetric displays[15,16] and optoelectronics.[22]

Though the functional diversity of RSLs is impressive, their range of use can be limited by conditions that promote dye−dye interactions. At high solution concentrations or in coating applications, dye−dye interactions can result in spectral shifts, quenching, and other unpredictable behavior. The exciton theory of dye−dye interactions originally developed by Kasha[24,25] and recently expanded by Spano[26−28] can serve as a theoretical tool relating dye aggregate behavior to photophysical properties. Exciton theory predicts the existence of H dimers (π-stacking of xanthene cores with parallel transition dipoles) or J dimers (offset xanthene cores and transition dipoles) in dye−dye interactions (Figure 2). H dimers typically exhibit hypsochromic absorbance and quenched fluorescence, while J dimers exhibit bathochromic absorbance and emission.[24,25] In concentrated solutions or in surface coatings, aggregates can be formed to a much greater extent than dimers, and domains can form of variable H/J interactive behavior.[26−28] Thus, there has been interest in studying rhodamine aggregation in solution and on surfaces in relation to exciton theory.[1,2,29−34] These studies have found clear evidence of pronounced spectral shifts and quenching that can be quantitatively difficult to predict.

https://doi.org/10.1021/acs.jpca.2c02665
J. Phys. Chem. A 2022, 126, 4211−4220

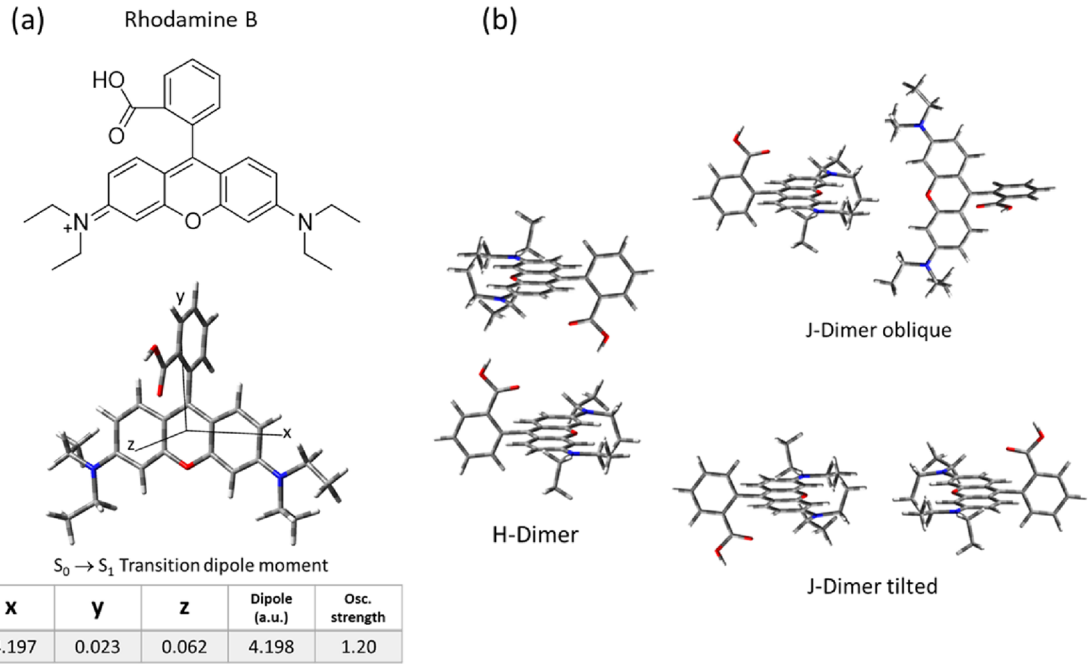

$S_0 \rightarrow S_1$ Transition dipole moment

x	y	z	Dipole (a.u.)	Osc. strength
-4.197	0.023	0.062	4.198	1.20

Figure 2. (a) Rhodamine B (top) with a stick structure, axes, and data table (bottom) indicating the orientation and size of the calculated transition dipole moment. (b) Potential Intermolecular orientations for H and J dimers of rhodamine B, as suggested by the work of Filatov et al.[29]

In this work, we report the synthesis and characterization of a rhodamine B dimer ($\mathbf{RB_2}$) in which we use *p*-phenylenediamine to create amide bonds with the carboxylic acid of two rhodamine B molecules, forming dual spirolactam moieties (Figure 1b). To our knowledge, this is the first covalently linked dimer of rhodamine B featuring spirolactam motifs. The phenyl moiety of the linker was chosen for structural rigidity and planarity; it was hypothesized such a linker would greatly constrict H/J interaction of the rhodamine B monomers, depending on the open−closed states of the spirolactam groups (both amides open, $\mathbf{RA_2}$, one open and one closed in spirocyclic form, **RSL-A**, and both closed, $\mathbf{RSL_2}$). Figure 3 exhibits the computationally derived lowest energy conformers of the three dimer species potentially participating in the overall equilibrium. As can be seen, the xanthene cores in these conformers might be predicted to have H or J dimer interactions based on their spatial proximity and relative orientations. It should be noted that these lowest energy conformers were not very energetically separated (∼1 kcal/mol) from conformers of varying xanthene orientations. Thus, there are potentially a wide variety of relative xanthene conformations at equilibrium in dimer solutions, making overall H or J dimer behavior difficult to predict. In addition, it was predicted that the equilibrium between the three states could be potentially controlled by pH or light activation. Results indicate that the dimer equilibrium not only favors the $\mathbf{RSL_2}$ form in most solvation environments but it also exhibits sensitivity to pH and UV illumination. Unlike previously reported RSLs, the $\mathbf{RSL_2}$ state of the dimer exhibits solvatochromic emissive behavior centered in the blue region of the spectrum, while the open forms exhibit fluorescence more typical of open-form RSLs. The open form spectral signature is slightly bathochromic relative to rhodamine B, indicating possible J-type interactions between the rhodamine B subunits of the dimer. The surprising color-switching of the dimer raises the possibility of applications that move beyond the on/off functionality of traditional RSLs.

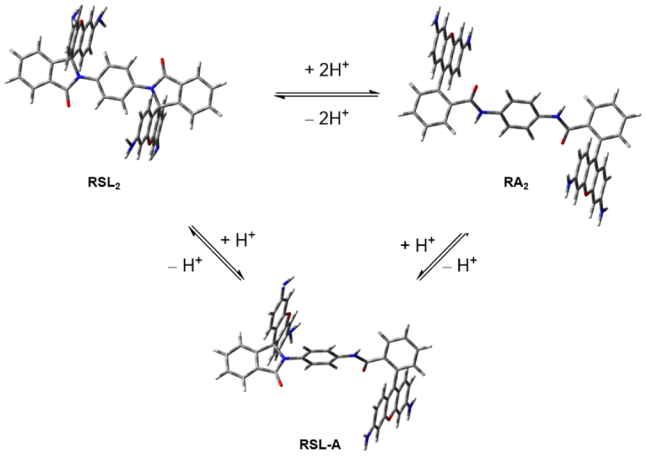

Figure 3. Computationally derived lowest energy conformers of the three dimeric species potentially present in solution at equilibrium.

METHODS

Materials. The following reagents were obtained from the vendors indicated and used without further purification: Rhodamine B (Sigma Life Sciences), *p*-phenylenediamine (Acros), *N*-(3-dimethylaminopropyl)-*N*′-ethylcarbodiimide hydrochloride (EDC·HCl) (Oakwood), 1-hydroxybenzotriazole hydrate (HOBt·H_2O) (CreoSalus), dichloromethane (OmniSolv), methanol (OmniSolv), 3-methyl-1-phenylindolin-2-one (MPO) (Alfa Aesar), and silica gel (Sorbtech). *N*,*N*′-(1,4-phenylene)dibenzamide (NPD) was prepared according to a literature procedure.[35] Flash chromatography was performed on a Teledyne CombiFlash NextGen 300+ flash purification system. NMR spectra were recorded using a JEOL ECZ-400S NMR spectrometer. Mass spectrometry data was acquired on a Shimadzu LCMS-8045. Elemental analysis was performed by Atlantic Microlab.

https://doi.org/10.1021/acs.jpca.2c02665
J. Phys. Chem. A 2022, 126, 4211−4220

Synthesis of 2,2″-(1,4-Phenylene)bis(3′,6′-bis(diethylamino)spiro[isoindoline-1,9′-xanthen]-3-one) (RSL_2). To a 100-mL round-bottom flask was added 0.906 g (1.89 mmol, 2.11 equiv) of rhodamine B, 0.289 g (2.14 mmol, 2.39 equiv) of 1-hydroxybenzotriazole hydrate ($HOBt·H_2O$), and 20 mL of dichloromethane (DCM). The reaction was stirred for 5 min, and 0.412 g (2.14 mmol, 2.39 equiv) of *N*-(3-dimethylaminopropyl)-*N*′-ethylcarbodiimide hydrochloride (EDC·HCl) was added and stirred for 30 min before adding 0.0967 g (0.894 mmol) *of p*-phenylenediamine. The flask was capped with a rubber septum, and the reaction was allowed to stir at room temperature overnight. The solution was washed with 50 mL of 1 M NaOH. The NaOH portion was then extracted with dichloromethane until it was light pink. The combined organic fractions were washed with 50 mL of brine, dried with sodium sulfate, and concentrated. The residue was purified by column chromatography on basic alumina using a gradient of 50−100% dichloromethane in heptanes to afford a white solid (198 mg, 0.207 mmol, 23% yield). ^{1}H NMR (400 MHz, dichloromethane-d_2) δ 7.90−7.83 (m, 2H), 7.50−7.36 (m, 4H), 6.95 (dd, J = 5.8, 2.4 Hz, 2H), 6.76 (s, 4H), 6.53 (d, J = 8.7 Hz, 4H), 6.32−6.18 (m, 8H), 3.28 (q, J = 7.1 Hz, 16H), 1.10 (t, J = 7.0 Hz, 24H). ^{13}C NMR (101 MHz, dichloromethane-d_2) δ 167.86, 154.32, 152.74, 148.87, 135.11, 132.96, 129.73, 128.43, 128.04, 126.00, 123.44, 123.18, 108.02, 105.87, 97.76, 67.04, 44.29, 12.38. Mass spec (ESI) for $C_{62}H_{65}N_6O_4$ (M + H): Calcd 957.5, found 957.4. Elemental analysis calculated for $C_{62}H_{64}N_6O_4$: C 77.80, H 6.74, N 8.78; found 76.75, H 6.82, N 8.32.

Absorbance and Fluorescence Studies. Absorbance and fluorescence excitation−emission matrix (EEM) measurements were made on an Agilent Cary 60 UV−VIS and a Shimadzu RF-6000 spectrofluorophotometer, respectively. Stock solutions of the dimer, rhodamine B, and aromatic controls (MPO/NPD) were made in DCM (dimer and aromatic controls), 2 M HCl/DMSO (acidified dimer), and EtOH (rhodamine B), respectively, at ∼mM concentrations and then diluted to 50 μM final concentrations in one of the solvents listed in Table 1, followed by thorough vortexing to ensure well-mixed final solutions. Fluorescence EEM measurements are affected by Rayleigh and Raman scattering, which can interfere with the analysis of the EEM spectra.[36] To minimize scattering contributions to spectra, a high-scattering blank was made by suspending 1.5 μm Si microspheres (Thermo Scientific) in water and subsequently run on the spectrofluorophotometer to obtain scatter blanks. The blank spectra consisted of a prominent scattering signal, with a background level signal outside of scattering regions. Spectra of fluorescence samples were then corrected by employing a logic test versus the scatter blank: in regions where signal intensity of the scatter blank was significantly higher than the sample, the signal was set to background levels, and in areas of sample spectrum in which the sample signal was higher than the blank scatter, the signal was left undisturbed. Examples of the blank and sample spectra (pre and post correction) are presented in the Supporting Information. Once corrected EEM measurements were obtained, integrated excitation and emission spectra were obtained by integrating all signals at each excitation or emission wavelength, respectively. The integration procedure is also outlined in more detail in the Supporting Information.

Table 1. List of Solvents Used in This Study, with Corresponding Hydrophobicity Ranked Using ET(30)[a] Values

solvent	ET(30)
H_2O	63.1
75% H_2O/25% MeCN	58.7
50% H_2O/50% MeCN	54.4
25% H_2O/75% MeCN	50.0
MeCN	45.6
DMSO	45.1
DCM	40.7
THF	37.4
hexane	31

[a]ET(30) values obtained from refs 37, 38.

Crystallographic Methods. A single-crystal specimen of $[C_{62}H_{68}N_6O_4][Cl]_4$-6 DMSO (colorless) and $[C_{62}H_{68}N_6O_4]$-$[Cl]_4$-H_2O (pink) forms was used for the X-ray crystallographic analysis. The X-ray intensity data were measured at 194 K on a Bruker APEX CCD system equipped with a sealed X-ray tube (Mo Kα, λ = 0.71073 Å) and a graphite monochromator. Both structures were solved and refined using the Bruker APEX/SHELXTL software package in space group *P*-1 (No. 2). The structure of the "colorless" form contained one $[C_{62}H_{68}N_6O_4][Cl]_4$-6 DMSO formula unit per unit cell in which two of the three crystallographically independent DMSO solvent molecules are disordered. The structure of the "pink" form contained two $[C_{62}H_{68}N_6O_4]$-$[Cl]_4$-H_2O formula units per unit cell in which each $[C_{62}H_{68}N_6O_4]^{4+}$ cation occupies a crystallographic inversion center. Complete crystallographic details are provided in the Supporting Information.

CCDC 2150573 and 2150574 contain the supplementary crystallographic data for this paper. These data can be obtained free of charge via www.ccdc.cam.ac.uk/data_request/cif, or by emailing to data_request@ccdc.cam.ac.uk, or by contacting The Cambridge Crystallographic Data Centre, 12 Union Road, Cambridge CB2 1EZ, UK; fax: +44 1223 336033.

Computational Details. The geometries of all modeled compounds were optimized at the M06-2X/6-31+G(d,p) level.[39] The stationary points on the potential energy surface were confirmed with frequency calculations. The UV−vis absorption and emission data were calculated using the TD-DFT method.[40] The solvent effects were taken into account using the Polarized Continuum Model (PCM).[41] The potential energy surface was examined through a relaxed scan, optimizing all other geometry parameters but the benzene linker dihedral angle that was kept fixed. All calculations were performed using the Gaussian 09 program package.[42]

RESULTS

Synthesis and Interconversion. The **RSL_2** dimer was synthesized by coupling rhodamine B chloride to *p*-phenylenediamine using the peptide coupling reagents HOBt and EDC·HCl. After basic extraction and purification by flash chromatography on basic alumina, the **RSL_2** dimer was isolated as a colorless solid. The ^{13}C NMR spectrum confirms the closed structure by the clear peak at 67 ppm, indicative of the quaternary spirolactam.[8,13] **RSL_2** has a limited solubility profile. Only chlorinated solvents such as dichloromethane and chloroform dissolve it well, whereas it is sparingly soluble in most organic solvents such as DMSO and THF. However, the

https://doi.org/10.1021/acs.jpca.2c02665
J. Phys. Chem. A 2022, 126, 4211−4220

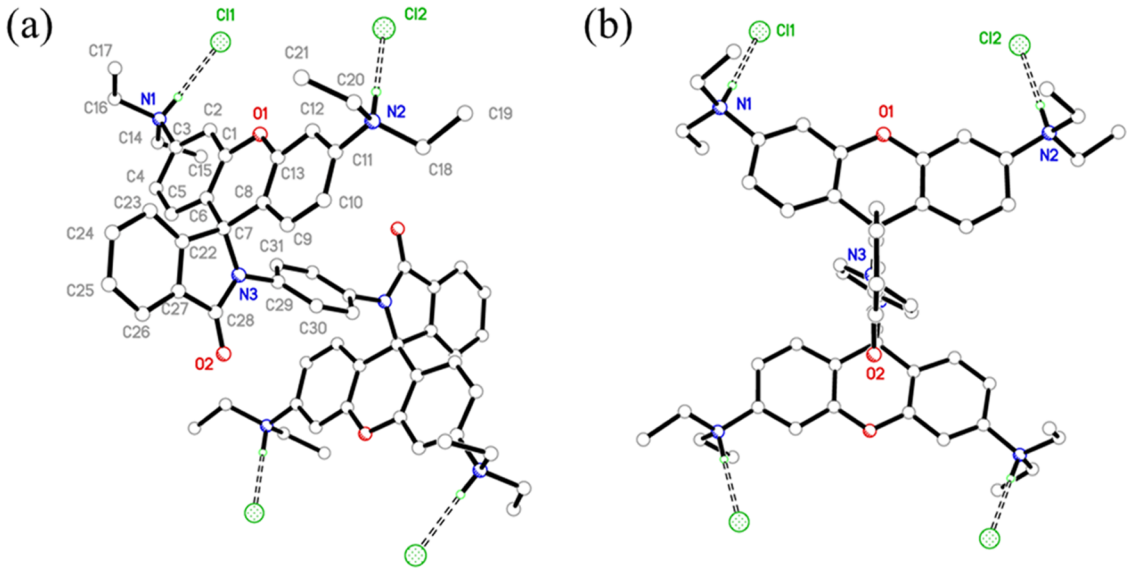

Figure 4. Two different views of the crystal structure obtained for **RSL_2-4HCl**. (a) Molecular structure and naming scheme for the asymmetric unit of the $[C_{62}H_{68}N_6O_4]^{4+}$ ion in crystalline $[C_{62}H_{68}N_6O_4][Cl]_4$-6 DMSO. (b) Alternative view of the dimer showing the protonated diethyl amines involved in hydrogen bonding with chloride counter ions.

RSL_2 solutions in chlorinated solvents develop a pink color with time, presumably due to the formation of ring-opened **RA_2** or **RSL-A** in the slightly acidic solvents. This color change is instantaneous in the case of chloroform and over a few hours in the case of dichloromethane. For these reasons, dichloromethane was chosen as the solution for **RSL_2**, but solutions were prepared immediately prior to use.

To prepare open forms for NMR analysis, **RSL_2** was reacted with 20% w/w DCl in D_2O and diluted with DMSO-d_6. The solution was bright pink, as would be expected for an open form of the xanthene moiety, and ^{1}H NMR indicates quantitative conversion to a new chemical species by the downfield shift of the xanthene signals and an upfield shift of the singlet from the benzene linker (see Figure S4). The signal integration ratios, the appearance of the benzene linker, and the number of ^{13}C NMR signals (Figure S5) are all consistent with a symmetric structure rather than the one-open/one-closed **RSL-A**. The quaternary spirolactam peak is still evident at 66 ppm in the ^{13}C NMR, indicating that the predominant species is protonated **RSL_2** formed from protonation of the diethylamine moieties on the xanthene rings, rather than **RA_2** or **RSL-A**. Because the quantum efficiency of the ring-opened species should be quite high as evidenced by other RSLs, it is reasonable that this species could be observable optically but not by NMR.

This structural determination is further supported by X-ray crystallographic analysis. Over a period of weeks, crystals are obtained from a solution of **RSL_2** that had been reacted with concentrated HCl and diluted with DMSO. The obtained crystal structure has a unit formula of $[C_{62}H_{68}N_6O_4][Cl]_4$ - 6 DMSO (**RSL_2-4HCl**) and shows protonation of the four diethylamine moieties, while the spiroisoindolone structure remains intact (Figure 4a). In the unit cell, **RSL_2-4HCl** sits on the crystallographic inversion center at (1/2, 1/2, 1/2) in the unit cell. The planes of the xanthene rings are 7.654 Å from each other, and they sit essentially perpendicular to the spiroisoindolone, with an angle of 88.86°. The perpendicular distance between planes of the two spiroisoindolones is 0.26 Å, and the planes are angled 60.47° to the plane of the benzene linker (Figure 4b). While the supernatant solution is pink, the crystal is colorless, which is consistent with the spirolactam form present.

Interestingly, once the crystal was removed from the nitrogen cold stream on the diffractometer and left at ambient conditions, it underwent a phase transformation as a pink color developed at the outer edges of the crystal and gradually moved inward over a period of a day (see Figure S6). Surprisingly, the pink crystal still produces an X-ray diffraction pattern suitable for characterization, though of lower quality than before (see the Supporting Information). This structure maintains the closed **RSL_2-4HCl** structure, though the DMSO solvent molecules have been replaced by water, and the unit cell is now composed of two **RSL_2-4HCl** formula units. The distances and angles between planes have shifted slightly. The spacing between the xanthene planes has decreased to 7.483 and 6.937 Å, while the spacing between the spiroisoindolone planes has increased to 1.607 and 1.498 Å for the two crystallographically independent dimers, respectively. The angles between the xanthene and spiroisoindolone planes are still essentially perpendicular at 90.16 and 84.74° for the dimers, respectively, while the angles between the spiroisoindolone and the benzene linker in the two formula units are now 50.99 and 54.53°, respectively. Further experimentation with colorless crystals has shown that exposure to a humid environment can reproducibly produce a color change within a matter of minutes. It is possible that the water displaces the DMSO solvent and facilitates a small amount of proton transfers to cause a small population of molecules to ring-open and display the observed color change.

Taken together, the ^{13}C NMR data and the crystallographic data point to an equilibrium between **RSL_2** and open forms that exists, as evidenced by the color change but which is heavily favored to the closed **RSL_2** form. This is surprising, as we expected a dimer in which bulky xanthene rings crowd the linker interior would instead highly favor the open **RA_2** form, especially under acidic conditions.

Optical Characteristics. To explore the spectral characteristics of the dimer, we sought to manipulate the solution

https://doi.org/10.1021/acs.jpca.2c02665
J. Phys. Chem. A 2022, 126, 4211−4220

equilibria of the different forms by changing solvation conditions. As outlined above, **RSL$_2$** is believed to be the dominant form in the solutions tested, but appreciable amounts of open forms are formed in acidified DMSO. For this reason, two ∼5 mM dimer stock solutions were made using DCM and 2 M HCl/DMSO. The DCM stock solution was clear and colorless, while the 2 M HCl/DMSO dimer stock solution was bright pink. We hypothesized that consistent with other RSLs, colorless solutions would be dominated by the **RSL$_2$** form of the dimer and thus would exhibit very little fluorescence, while pinker solutions would exhibit rhodamine B-like fluorescence due to open forms of the dimer being present.[9,14] Fluorescence absorption (dotted lines) and emission (solid lines) spectra are shown for 50 μM solutions created from the 5 mM DCM (Figure 5a) and 2 M HCl/DMSO dimer stocks (Figure 5b) in three representative solvents of varying hydrophobicity: 50:50 water/MeCN, DMSO, and DCM (red, green, blue lines, respectively). The inset in the spectra figures are photos of the respective sample solutions excited at 305 and 365 nm. A wider range of solvent polarities were tested, and their spectra and inset photos are shown in Figures S10 and S11. All spectra exhibited prominent UV fluorescence excitation peaks (∼300 nm excitation max), with other notable excitation peaks in the region typical of rhodamine B (∼560 nm). As expected, sample solutions made from the 2 M HCl/DMSO dimer stock exhibited much more prominent rhodamine B-like excitation, likely due to the presence of HCl acid (∼20 mM in sample solutions).

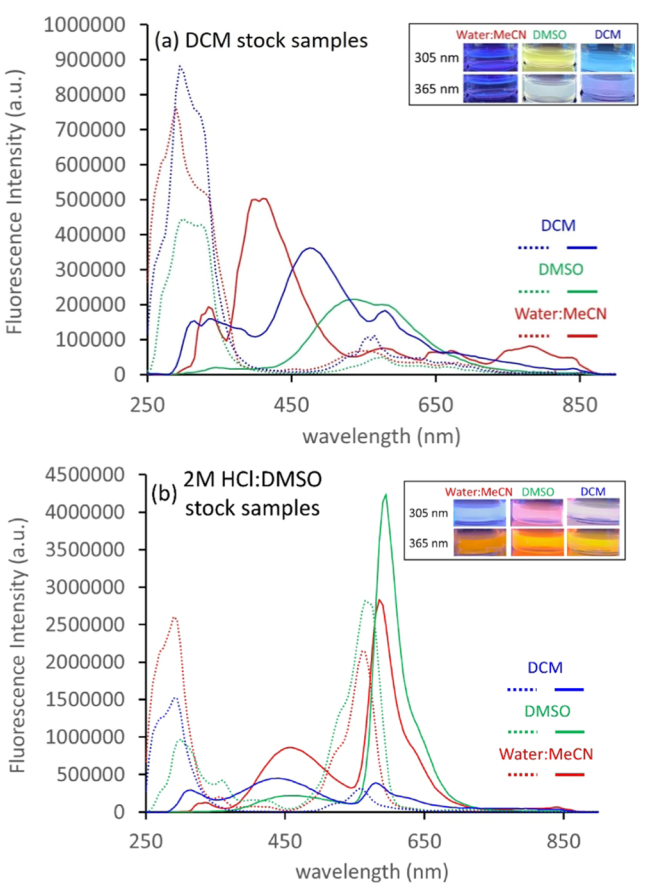

Figure 5. Fluorescence excitation (dotted lines) and emission (solid lines) spectra of 50 μM dimer sample solutions in three example solvents: DCM (blue lines), DMSO (green lines), and 50:50 water/MeCN (red lines). (a) Spectra generated from samples diluted from a DCM stock of the dimer. The inset shows pictures of the same 3 mL solutions used to collect the spectra under UV lamp illumination at 305 and 365 nm. (b) Spectra generated from samples diluted from a 2 M HCl/DMSO stock of the dimer, resulting in sample solutions containing ∼20 mM HCl. The inset shows pictures of the same 3 mL solutions used to collect the b spectra under UV lamp illumination at 305 and 365 nm.

Given the NMR and crystallographic data that indicates **RSL$_2$** is a doubly closed spirolactam form of the dimer, it is quite surprising that there is appreciable fluorescence emission from the clear solutions across a wide range of solvent polarities (Figure 5a). In the polar water−MeCN mixture diluted from DCM dimer stock, the sample exhibited an emission max of 410 nm, with a secondary peak at 335 nm and a relatively minor peak at 580 nm near the typical rhodamine B emission max, with a series of shoulders venturing farther into the red part of the spectrum. In medium-polarity DMSO, the peak at 335 nm is barely visible, the peak at 410 nm red-shifts to an emission max of 535 nm, and the shoulder at 580 nm becomes more prominent. In DCM, the most hydrophobic solvent system used, the 335 nm peak is once again more prominent, the middle peak blue-shifts to 474 nm, and the shoulder is now located at 575 nm. It is notable that these spectral profiles differ markedly from typical rhodamine B spirolactams, which uniformly exhibit on/off spectral behavior with a peak identical to rhodamine B.[9,14,16] In **RSL$_2$**, the apparent solvatochromic peak which shifts between an emission max of 410 and 535 nm is the dominant fluorescence emission peak of dimer solutions, regardless of the solvent. We hypothesize that the solvatochromic peak is due to the closed **RSL$_2$** form of the dimer, with the 580 nm contributions to the spectra indicating a contribution from **RA$_2$** (or possibly **RSL-A**) in solution equilibrium. We also observe this blue fluorescence when the colorless crystals discussed above are irradiated with UV light, indicating that this solvatochromic peak is observed in the solid state as well.

By comparison, the samples created from the 2 M HCl/DMSO dimer stock exhibited a pink color across a wide range of solvation conditions (Figure 5b). As expected from the pink color, acidified dimer sample solutions exhibited much more prominent orange emission peaks (∼585 to 590 nm) that closely resemble rhodamine B fluorescence but are slightly bathochromic, indicating possible J-type interactions between the subunits of the dimer (control rhodamine B spectra, with comparison to the orange dimer peak, can be found in Figure S12). Again, rhodamine spirolactams are known to ring-open and exhibit rhodamine B-like fluorescence in acidic conditions, so it is not surprising we see such behavior.[9,14] However, like the dimer solutions diluted from the DCM stock, the acidified dimer samples exhibit significant blue emission (460 nm max in water/MeCN and DMSO, 440 nm max in DCM). Notably, the intensity ratios between the orange and blue peaks vary with the solvents, with the orange peak being most dominant in the DMSO solvent and the blue peak dominating the DCM solvent. Once again, we hypothesize that the spectra indicate an equilibrium between the **RSL$_2$** ↔ **RSL-A** ↔ **RA$_2$** species, which contribute to the blue (**RSL$_2$**) and orange emission peaks (**RSL-A**, **RA$_2$**), respectively. The blue emission peak exhibits less color-shifting behavior across the range of solvents tested when compared to the nonacidified dimer samples. It is hypothesized that the significant presence of acid (∼20 mM in fluorescence samples) reduces the heterogeneity in the

https://doi.org/10.1021/acs.jpca.2c02665
J. Phys. Chem. A 2022, 126, 4211−4220

solvation environment for the acidified dimer samples, thus decreasing the spectral shifts with respect to the solvent. Like the pink solutions, when the pink crystals were irradiated by UV light, we observe both orange and blue fluorescence, which we hypothesize is due to the presence of both open and closed forms in an equilibrium (see Figure S7).

Absorbance measurements for both the dimer and acidified dimer samples were performed as well to see if the UV−Vis spectra departed significantly from fluorescence excitation spectra. There were no significant absorption peaks outside of fluorescence excitation regions. These absorbance spectra can be seen in Figure S12.

UV Sensitivity. Given our hypothesis that the **RSL$_2$** dimer exhibits the typical rhodamine spirolactam ring-opening behavior in acidic solution, we also wanted to investigate potential ring-opening under UV illumination. UV light is known to cause ring-opening in rhodamine spirolactams, and longer UV exposure times would be expected to convert more **RSL$_2$** into open forms.[15,16] Figure 6 shows spectra obtained from a 50 μM solution of a dimer sample in DCM after varying exposures to 305 nm light (excitation: dotted colored lines, emission: solid colored lines). The solution was exposed in 15 s intervals, from no exposure (red lines) to 2 min (purple lines). There is a clear trend in the spectra of the emission peak centered at ∼475 nm (blue fluorescence) decreasing with prolonged exposure, with the peak at ∼585 nm (orange fluorescence) showing a corresponding increase. This is consistent with the hypothesis that the blue fluorescence is indicative of **RSL$_2$** in solution, while the orange fluorescence is contributed by one of the open forms. Also shown is an excitation spectrum (black circles) and emission spectrum (black triangles) of the same DCM solution after the 2 min of UV exposure and subsequent storage in the dark at room temperature for 5 days. It can be seen that the solution has largely reverted to the same fluorescence profile as was observed in the original, unexposed **RSL$_2$** sample. This provides evidence that the UV illumination is not causing unforeseen photochemistry in the sample and is merely driving equilibrium toward open forms in a solvation environment that largely favors **RSL$_2$**.

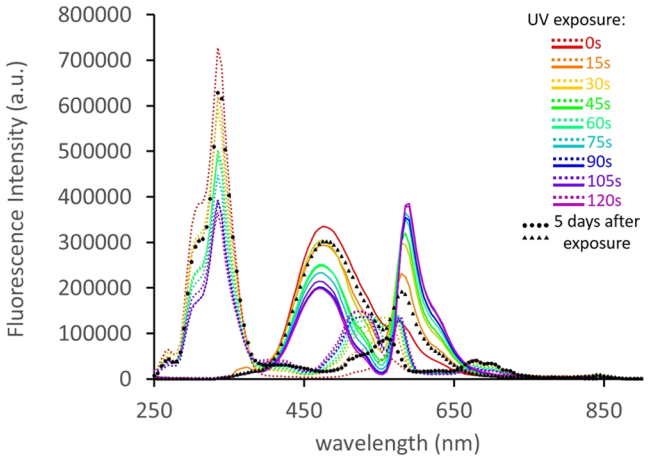

Figure 6. Fluorescence excitation and emission spectra of a 50 μM dimer sample in DCM solution exposed to varying amounts of 305 nm UV light. Colored lines represent fluorescence excitation spectra (dotted lines) and emission spectra (solid lines) as the sample was subjected to increasing exposures in 15 s increments. Black circles (excitation) and black triangles (emission) represent the same sample stored 5 days at room temperature in the dark after the longest exposure of 120 s.

Aromatic Control Spectra to Investigate Possible Sample Contamination. In an effort to investigate the source of the solvatochromic emission peak present in solutions believed to contain predominantly the **RSL$_2$** form of the dimer, we explored the spectral characteristics of two aromatic molecules, MPO and NPD. These two molecules were chosen due to their structural similarity to linker-associated motifs present in the dimer. If the spectra obtained from these two controls closely mimicked the solvatochromic portion of dimer spectra, it could indicate one of two possibilities: either the closed linker structure could be contributing to the solvatochromic fluorescence of the dimer, or dimer solutions are contaminated with some linker-related species. We feel that sample contamination is highly unlikely due to the white crystalline appearance of the solid dimer, the well-resolved NMR spectra, the absence of impurities detectable by HPLC (see Figures S1−S3), and the interconversion between the orange and blue emission peaks in the UV exposure experiments. Thus, we thought it more likely that spectral similarities between these controls and the dimer spectra would indicate possible linker contributions to dimer spectra. The excitation and emission spectra of these two compounds in the same solvents used in Figure 5a,b can be seen in Figure 7a (MPO) and 7b (NPD). The two controls had very similar spectra, with fluorescence emission evident at ∼335 and ∼650 nm. There was spectral emission from dimer samples in the ∼335 and ∼650 nm regions in some of the solvents tested. For instance, the 50 μM DCM sample in Figure 5a exhibits fluorescence emission in these regions. In addition, the hexane samples for both dimer stocks much more strongly resembled the spectra of the aromatic controls, as can be seen in Figures S10 and S11. However, the spectra of the control molecules do not present peaks similar to the prominent solvatochromic peak of the dimer, which argues against the hypothesis of these structural motifs contributing to said peak. Given that the aromatic controls exhibited consistent spectral characteristics in a wide range of hydrophobicities and that these signatures are not evident in most dimer spectra, we hypothesize that the similar dimer peaks are not due to contamination but rather due to the impact of the solvation environment on the fluorescent moieties of the dimer.

Computational Modeling. To further understand the properties of the dimers, **RSL$_2$**, **RSL-A**, and **RA$_2$** were modeled in DCM. The three structures are very close energetically, with energy differences of less than 1 kcal/mol. This is consistent with the hypothesis that they coexist in the solution. Further investigations point toward a very flat potential energy surface of **RSL$_2$** with respect to rotation of the benzene linker with respect to the spiroisoindolone plane (Figure S15). The minimum corresponds to an angle of 76°, which is in good agreement with the experimental X-ray structure data, especially taking into account the fact that the computational modeling was performed in solution. We will refer to this structure as **RSL$_2$** (θ = 76°). The maximum corresponds to **RSL$_2$** (θ = 0°) or a planar spiroisoindolone−benzene−spiroisoindolone structure. Vibrational analysis indicates that this maximum is a transition state that connects the two minima **RSL$_2$** (θ = 76°) and **RSL$_2$** (θ = −76°). The barrier for rotation of the benzene linker is very small, less than 3 kcal/

https://doi.org/10.1021/acs.jpca.2c02665
J. Phys. Chem. A 2022, 126, 4211−4220

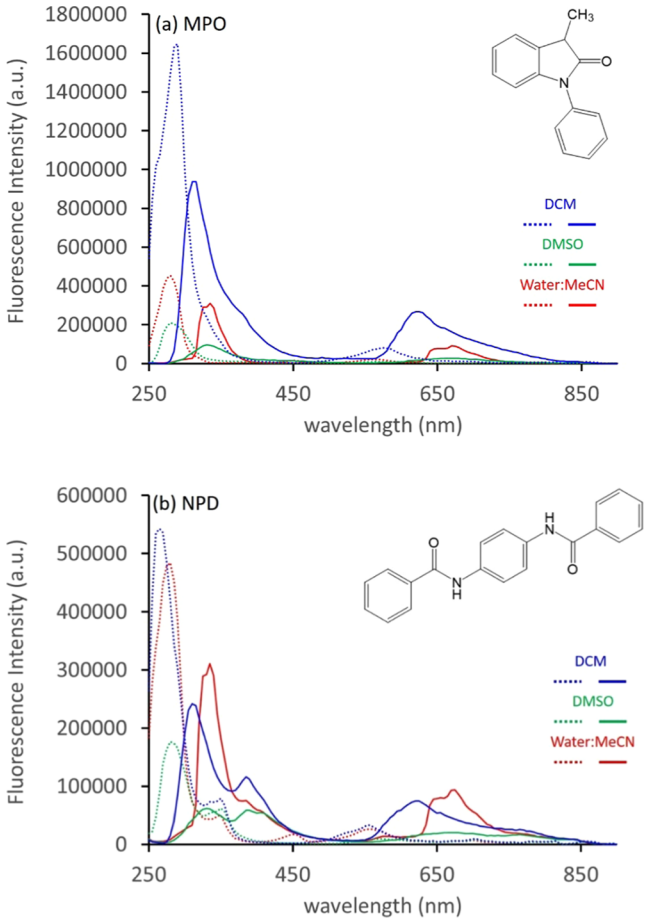

Figure 7. Spectra of 50 μM MPO, NPD controls in the same three solvents used in Figure 5a,b. Insets show their respective structures. (a) Fluorescence excitation and emission profiles of the MPO control. (b) Fluorescence excitation and emission profiles of the NPD control. Emission spectral features do not overlap with the two main emission peaks for the dimer. However, there is some spectral overlap with less prominent peaks in the dimer spectra.

mol. Since it is significantly less than 20 kcal/mol, our calculations suggest that at room temperature the benzene linker rotates freely in the solution.

With regards to the solvatochromic peak, TD-DFT calculations of the UV−vis absorption and emission spectra of **RSL$_2$** (θ = 76°) indicate mixed transitions and no fluorescence. However, the planarity of the spiroisoindolone−benzene−spiroisoindolone structure in **RSL$_2$** (θ = 0°) allows for significant delocalization of the electron density along this plane. Figure S16 compares the frontier molecular orbitals of **RSL$_2$** (θ = 76°) and **RSL$_2$** (θ = 0°). In **RSL$_2$** (θ = 76°), the LUMO is delocalized, but the HOMO is localized on the two rhodamine B subunits, resulting in no fluorescence as expected for the closed structure. In **RSL$_2$** (θ = 0°), a new HOMO orbital appears, and both HOMO and LUMO are delocalized across the spiroisoindolone−benzene−spiroisoindolone plane. The HOMO−LUMO gap significantly decreases, and the structure's fluorescence is hypsochromic by 87 nm compared to rhodamine B. This is in good agreement with the experimentally observed shift of around 100 nm.

DISCUSSION

As previously reported, the equilibrium between closed and opened forms of RSLs is influenced by the solvation environment, size of prosthetic groups, and the electron-withdrawing/donating nature of those groups.[9,14,16] Given the relatively large size of a rhodamine B prosthetic group in relation to the size of prosthetic groups in previous studies, we initially hypothesized that the doubly open form of the dimer would be favored in equilibrium due to steric effects. Data obtained from NMR, single-crystal X-ray diffraction, and fluorescence EEM spectroscopy all point toward the doubly closed form of the dimer being favored under most conditions. Given the propensity of rhodamine B to form intermolecular aggregates in solution at higher concentrations,[2,43,44] it is possible that the forced proximity of the rhodamine B subunits of the dimer encourages dimer stereochemistry, which promotes the closed form's intramolecular "aggregation."

The solvatochromic peak of **RSL$_2$** is surprising. One explanation for the solvatochromic emission of the closed-form is that the aromatic linker is responsible for the fluorescence. Though the linker-mimicking aromatic controls MPO and NPD exhibited fluorescence emission that did not resemble the solvatochromic peak, it is possible that the unique molecular environment of the linker, sandwiched between the two xanthene substituents, results in substantial emission-shifting of the linker's fluorescence. While the crystallographic and computational data both support a favored bond angle between the benzene linker and spiroisoindolone planes that should preclude fluorescence, the small barrier to rotation indicates that at any given time, a significant enough population of molecules may be present to lead the observed blue fluorescence. Indeed, this barrier is small enough that a small population of molecules may be able to adopt this conformation in the solid state of the colorless crystal at any given time. If the linker is responsible for the blue fluorescence emission, the solvatochromic aspect of this emission may be explained by conformational changes influencing solvent penetration into the areas of the dimer proximal to the linker.

On the other hand, intramolecular interactions could potentially also explain the presence of the solvatochromic peak; though the spirolactam disrupts the continuous conjugation of the xanthene cores, there are still a number of aromatic moieties in the closed form of the dimer. The number and proximity of the aromatic moieties could result in intramolecular interactions, leading to "aggregation"-induced emission. This might also explain the solvatochromic nature of the emission, as different solvation environments may result in conformational changes in the dimer's subunits, resulting in changing intramolecular spatial relationships between the aromatic moieties. Aggregation-induced spectral shifts related to the solvation environment have been observed previously for rhodamine-based probes, though not originating from closed lactone/lactam forms.[7] Such aggregation effects in the solid state could also explain the blue fluorescence observed in the colorless crystal when irradiated with UV light.

CONCLUSIONS

In this work, we report the synthesis and fluorescence characterization of a dimer of rhodamine B connected using a *p*-phenylenediamine linker, which results in a dual spirolactam motif. As with other RSLs, the dimer exhibited spirolactam sensitivity to both pH and UV illumination.

https://doi.org/10.1021/acs.jpca.2c02665
J. Phys. Chem. A 2022, 126, 4211−4220

Surprisingly, evidence suggests that the doubly closed form of the dimer exhibits solvatochromic fluorescence emission centered in the blue region of the spectrum. In addition, the evidence also suggests that the dimer equilibrium is heavily weighted toward the doubly closed form, regardless of the solvation environment. The NMR and crystallographic data indicate that the closed form of the dimer is dominant, with little to no signal indicating either of the open forms of the dimer. The primary evidence that ring-opening occurs is the pink solution color of the dimer in acidic or UV-exposed conditions and the corresponding rhodamine B-like fluorescence emission. It is possible that the pink form of the dimer could be either the singly open **RSL-A** form or the doubly open **RA_2** form, as it is unclear if there would be any spectral characteristics that differ appreciably between these two forms. The surprising equilibrium and fluorescence emission characteristics of the dimer lead to questions about how the structure of the linker influences both. In future work, we seek to investigate linker chemistry that influences the open−closed equilibrium, as well as the solvatochromic emission. We hypothesize that increasing the steric bulk of the linker may drive the dimer toward more open forms. In addition, changes to the aromaticity of the linker may drastically modify the solvatochromic emission of the dimer. If linker chemistry can fine-tune both the open−closed equilibrium and the solvation response of the dimers, it has the potential to expand the applicability of rhodamine spirolactam molecular sensing.

■ ASSOCIATED CONTENT

Supporting Information

The Supporting Information is available free of charge at https://pubs.acs.org/doi/10.1021/acs.jpca.2c02665.

Additional tables and figures related to ^{1}H NMR and ^{13}C NMR spectra of **RSL_2** and **RSL_2-4HCl**, HPLC traces of **RSL_2**, absorbance and fluorescence spectra in additional solvents and of rhodamine B and control molecules, and computational and crystallographic data (PDF)

Accession Codes

Single-crystal X-ray data are included and have been deposited at the Cambridge Crystallographic Data Centre under Deposition Nos. CCDC 2150573 and 2150574.

■ AUTHOR INFORMATION

Corresponding Authors

Pamela M. Lundin − *Department of Chemistry, High Point University, High Point, North Carolina 27268, United States;* orcid.org/0000-0002-6071-1440; Email: plundin@highpoint.edu

Keir H. Fogarty − *Department of Chemistry, High Point University, High Point, North Carolina 27268, United States;* orcid.org/0000-0001-8953-4778; Email: kfogarty@highpoint.edu

Authors

Brandy-Fey C. Stratton − *Department of Chemistry, High Point University, High Point, North Carolina 27268, United States*

Angelina J. Pierre − *Department of Chemistry, High Point University, High Point, North Carolina 27268, United States*

Elizabeth A. Riser − *Department of Chemistry, High Point University, High Point, North Carolina 27268, United States*

Nathan J. Grinalds − *Department of Chemistry, High Point University, High Point, North Carolina 27268, United States*

Charles W. Edwards − *Department of Chemistry, High Point University, High Point, North Carolina 27268, United States*

Anna M. Wohlwend − *Department of Chemistry, High Point University, High Point, North Carolina 27268, United States*

Jacob S. Bauer − *Department of Chemistry, High Point University, High Point, North Carolina 27268, United States*

Rachel J. Spera − *Department of Chemistry, High Point University, High Point, North Carolina 27268, United States*

Lauren S. Pferdmenges − *Department of Chemistry, High Point University, High Point, North Carolina 27268, United States*

Kaitlyn M. Griffith − *Department of Chemistry, High Point University, High Point, North Carolina 27268, United States*

Brandon W. Hunter − *Department of Chemistry, High Point University, High Point, North Carolina 27268, United States*

Petia Bobadova-Parvanova − *Department of Chemistry and Fermentation Sciences, Appalachian State University, Boone, North Carolina 28608, United States;* orcid.org/0000-0002-1965-419X

Cynthia S. Day − *Department of Chemistry, Wake Forest University, Winston Salem, North Carolina 27109, United States*

Complete contact information is available at: https://pubs.acs.org/10.1021/acs.jpca.2c02665

Author Contributions

A.J.P., E.A.R., C.W.E., L.S.P., and P.M.L. performed the synthesis, purifications, and synthetic characterizations. B.-F.C.S., N.J.G., A.M.W., J.S.B., R.J.S., K.M.G., B.W.H., and K.H.F. performed the optical measurements. C.S.D. collected and analyzed the crystallographic data. P.B.-P. collected and analyzed the computational data. The manuscript was written through contributions of all authors. All authors have given approval to the final version of the manuscript.

Funding

This work was supported by the National Science Foundation Major Research Instrumentation Program (CHE-1919685 to P.M.L.) and High Point University.

Notes

The authors declare no competing financial interest.

■ ACKNOWLEDGMENTS

P.M.L. and A.J.P. thank Alan Barber of Teledyne for assistance and helpful discussions.

■ REFERENCES

(1) Selwyn, J. E.; Steinfeld, J. I. Aggregation of equilibriums of xanthene dyes. *J. Phys. Chem. A* **1972**, *76*, 762−774.

(2) Valdes-Aguilera, O.; Neckers, D. C. Aggregation phenomena in xanthene dyes. *Acc. Chem. Res.* **1989**, *22*, 171−177.

(3) Arbeloa, I. L.; Ojeda, P. R. Dimeric states of rhodamine B. *Chem. Phys. Lett.* **1982**, *87*, 556−560.

(4) Snare, M. J.; Treloar, F. E.; Chiggino, K. P.; Thistlethwaite, P. J. The photophysics of rhodamine B. *J. Photochem.* **1982**, *18*, 335−346.

(5) Salleh, M. A. M.; Mahmoud, D. K.; Abdul Karim, W. A. W.; Idris, A. Cationic and anionic dye adsorption by agricultural solid wastes: A comprehensive review. *Desalination* **2011**, *280*, 1−13.

(6) Gong, Y.-J.; Zhang, M.-L.; Wang, B.-X.; Lv, Q.; Wang, Y.; Dong, W. A smart approach toward rhodamine spiro-ring derivatives sensing platform for lysosome-targetable imaging applications. *Sens. Actuators, B* **2019**, *283*, 239−246.

(7) Arsov, Z.; Urbancic, I.; Strancar, J. Aggregation-induced emission spectral shift as a measure of local concentration of a pH-activatable rhodamine-based smart probe. *Spectrochim. Acta, Part A* **2018**, *190*, 486−493.
(8) Best, Q. A.; Liu, C.; van Hoveln, P. D.; McCarroll, M. E.; Scott, C. N. Anilinomethylrhodamines: pH Sensitive Probes with Tunable Photophysical Properties by Substituent Effect. *J. Org. Chem.* **2013**, *78*, 10134−10143.
(9) Liu, C.; Best, Q. A.; Suarez, B.; Pertile, J.; McCarroll, M. E.; Scott, C. N. Cycloalkyl-AminoMethylRhodamines: pH Dependent Photophysical Properties Tuned by Cycloalkane Ring Size. *J. Fluoresc.* **2015**, *25*, 231−237.
(10) Di Paolo, M.; Boubeta, F. M.; Alday, J.; Torino, M. M.; Aramendia, P. F.; Suarez, S. A.; Bossi, M. L. Design and characterization of pH-sensitive spirorhodamine 6G probes with aliphatic substituents. *J. Photochem. Photobiol., A* **2019**, *384*, No. 112011.
(11) Min, L.; Li, X.; Zhang, W.; Zhang, X.; Zhang, Y.; Yu, H.; Xiao, Y. pKa modulation of rhodamine alkylamides by hydrogen-bond and application in bio-imaging. *Dyes Pigm.* **2021**, *188*, No. 109173.
(12) Yu, K.-K.; Li, K.; Hou, J.-T.; Yang, J.; Xie, Y.-M.; Yu, X.-Q. Rhodamine based pH-sensitive "intelligent" polymers as lysosome targeting probes and their imaging applications in vivo. *Polym. Chem.* **2014**, *5*, 5804−5812.
(13) Czaplyski, W. L.; Purnell, G. E.; Roberts, C. A.; Allred, R. M.; Harbron, E. J. Substituent effects on the turn-on kinetics of rhodamine-based fluorescent pH probes. *Org. Biomol. Chem.* **2014**, *12*, 526−533.
(14) Stratton, S. G.; Taumoefolau, G. H.; Purnell, G. E.; Rasooly, M.; Czaplyski, W. L.; Harbron, E. J. Tuning the pKa of Fluorescent Rhodamine pH Probes through Substituent Effects. *Chem. − Eur. J.* **2017**, *23*, 14064−14072.
(15) Patel, S. K.; Cao, J.; Lippert, A. R. A volumetric three-dimensional digital light photoactivatable dye display. *Nat. Commun.* **2017**, *8*, No. 15239.
(16) Li, B.; Haris, U.; Aljowni, M.; Nakatsuka, A.; Patel, S. K.; Lippert, A. R. Tuning the Photophysical Properties of Spirolactam Rhodamine Photoswitches. *Isr. J. Chem.* **2021**, *61*, 244−252.
(17) Belov, V. N.; Bossi, M. L.; Foelling, J.; Boyarskiy, V. P.; Hell, S. W. Rhodamine spiroamides for multicolor single-molecule switching fluorescent nanoscopy. *Chem. − Eur. J.* **2009**, *15*, 10762−10776.
(18) Mitronova, G. Y.; Belov, V. N.; Bossi, M. L.; Wurm, C. A.; Meyer, L.; Medda, R.; Moneron, G.; Bretschneider, S.; Eggeling, C.; Jakobs, S.; Hell, S. W. New Fluorinated Rhodamines for Optical Microscopy and Nanoscopy. *Chem. − Eur. J.* **2010**, *16*, 4477.
(19) Montenegro, H.; Di Paolo, M.; Capdevila, D.; Aramendia, P. F.; Bossi, M. L. The mechanism of the photochromic transformation of spirorhodamines. *Photochem. Photobiol. Sci.* **2012**, *11*, 1081−1086.
(20) Willwohl, H.; Wolfrum, J.; Gleiter, R. Kinetics and mechanism of the photochromism of N-phenyl-rhodaminelactame. *Laser Chem.* **1989**, *10*, 63−72.
(21) Halabi, E. A.; Pinotsi, D.; Rivera-Fuentes, P. Photoregulated fluxional fluorophores for live-cell super-resolution microscopy with no apparent photobleaching. *Nat. Commun.* **2019**, *10*, No. 1232.
(22) Wang, X.; Wang, S.; Gu, C.; Zhang, W.; Zheng, H.; Zhang, J.; Lu, G.; Zhang, Y.-M.; Li, M.; Zhang, S. X.-A. Reversible Bond/Cation-Coupled Electron Transfer on Phenylenediamine-Based Rhodamine B and Its Application on Electrochromism. *ACS Appl. Mater. Interfaces* **2017**, *9*, 20196−20204.
(23) Lee, M. K.; Rai, P.; Williams, J.; Twieg, R. J.; Moerner, W. E. Small-Molecule Labeling of Live Cell Surfaces for Three-Dimensional Super-Resolution Microscopy. *J. Am. Chem. Soc.* **2014**, *136*, 14003−14006.
(24) Kasha, M. Energy Transfer Mechanisms and the Molecular Exciton Model For Molecular Aggregates. *Radiat. Res.* **1963**, *20*, 55−70.
(25) Kasha, M.; Rawls, H. R.; El-Bayoumi, M. A. The exciton model in molecular spectroscopy. *Pure Appl. Chem.* **1965**, *11*, 371−392.
(26) Spano, F. C. The spectral signatures of frenkel polarons in H- And J-aggregates. *Acc. Chem. Res.* **2010**, *43*, 429−439.
(27) Hestand, N. J.; Spano, F. C. Expanded Theory of H- and J-Molecular Aggregates: The Effects of Vibronic Coupling and Intermolecular Charge Transfer. *Chem. Rev.* **2018**, *118*, 7069−7163.
(28) Hestand, N. J.; Spano, F. C. Molecular Aggregate Photophysics beyond the Kasha Model: Novel Design Principles for Organic Materials. *Acc. Chem. Res.* **2017**, *50*, 341−350.
(29) Setiawan, D.; Kazaryan, A.; Martoprawiro, M. A.; Filatov, M. A first principles study of fluorescence quenching in Rhodamine B dimers: how can quenching occur in dimeric species? *Phys. Chem. Chem. Phys.* **2010**, *12*, 11238−11244.
(30) Alhasani, M.; Gupta, A.; Euler, W. B. Modulation of the fluorescent properties of rhodamine 6G by Zn2+-doped PVDF films. *J. Lumin.* **2018**, *196*, 116−125.
(31) Chapman, M.; Mullen, M.; Novoa-Ortega, E.; Alhasani, M.; Elman, J. F.; Euler, W. B. Structural Evolution of Ultrathin Films of Rhodamine 6G on Glass. *J. Phys. Chem. C* **2016**, *120*, 8289−8297.
(32) Mullen, M.; Fontaine, N.; Euler, W. B. A Spectroscopic Study of Xanthene Dyes on a Polystyrene Surface: an Investigation of Ion-π Interactions at Polymer Interfaces. *J. Fluoresc.* **2020**, *30*, 811−818.
(33) Chapman, M.; Euler, W. B. Rhodamine 6G Structural Changes in Water/Ethanol Mixed Solvent. *J. Fluoresc.* **2018**, *28*, 1431−1437.
(34) Fujii, T.; Nishikiori, H.; Tamura, T. Absorption spectra of rhodamine B dimers in dip-coated thin films prepared by the sol-gel method. *Chem. Phys. Lett.* **1995**, *233*, 424−429.
(35) Chen, L.; Huang, G.-L.; Lu, M.-H.; Zhang, Y.-X.; Xu, J.; Bai, S.-P. Amide derivatives of Gallic acid: Design, synthesis and evaluation of inhibitory activities against in vitro α-synuclein aggregation. *Bioorg. Med. Chem.* **2020**, *28*, No. 115596.
(36) Bahram, M.; Bro, R.; Stedmon, C.; Afkhami, A. Handling of Rayleigh and Raman scatter for PARAFAC modeling of fluorescence data using interpolation. *J. Chemom.* **2006**, *20*, 99−105.
(37) Mancini, P. M. E.; Terenzani, A.; Gasparri, M. G.; Vottero, L. R. Determination of the empirical polarity parameter ET(30) for binary solvent mixtures. *J. Phys. Org. Chem.* **1995**, *8*, 617−625.
(38) Reichardt, C. *Solvents and Solvent Effects in Organic Chemistry*, 3rd ed.; John Wiley & Sons, 2003.
(39) Zhao, Y.; Truhlar, D. G. The M06 suite of density functionals for main group thermochemistry, thermochemical kinetics, noncovalent interactions, excited states, and transition elements: two new functionals and systematic testing of four M06-class functionals and 12 other functionals. *Theor. Chem. Acc.* **2008**, *120*, 215−241.
(40) Bauernschmitt, R.; Ahlrichs, R. Treatment of electronic excitations within the adiabatic approximation of time dependent density functional theory. *Chem. Phys. Lett.* **1996**, *256*, 454−464.
(41) Tomasi, J.; Mennucci, B.; Cammi, R. Quantum Mechanical Continuum Solvation Models. *Chem. Rev.* **2005**, *105*, 2999−3093.
(42) Frisch, M. J. T.; G, W.; Schlegel, H. B.; Scuseria, G. E.; Robb, M. A.; Cheeseman, J. R.; Scalmani, G.; Barone, V.; Mennucci, B.; Petersson, G. A.et al.*Gaussian 09*, revision D.01; Gaussian, Inc.: Wallingford, CT, 2009.
(43) Arbeloa, F.; Ruiz Ojeda, P.; Lopez Arbeloa, I. On the aggregation of rhodamine B in ethanol. *Chem. Phys. Lett.* **1988**, *148*, 253−258.
(44) Halterman, R. L.; Moore, J. L.; Yip, W. T. Cucurbit[7]uril Disrupts Aggregate Formation Between Rhodamine B Dyes Covalently Attached to Glass Substrates. *J. Fluoresc.* **2011**, *21*, 1467−1478.

https://doi.org/10.1021/acs.jpca.2c02665
J. Phys. Chem. A 2022, 126, 4211−4220